EPJ Web of Conferences **233**, 04003 (2020) https://doi.org/10.1051/epjconf/202023304003
CMPNC 2019

Electrical response of $La_{2/3-x}Li_{3x}TiO_3$ ceramics obtained by spark plasma sintering

J. Silva-Pereira [1], *F.* Guerrero [1], *Y.* Romaguera-Barcelay [1], *L.* Aguilera[2], *R. S.* Silva[3], *J.* Anglada- Rivera[4], *N. C.* Pillajo[5], *A.* Almeida[6], *J.* Agostinho Moreira[6] *and Y.* Leyet [1, 5]

[1]Departamento de Física, Universidade Federal do Amazonas, 69077-000, Manaus, AM, Brasil
[2] Departamento de Química, Universidade Federal do Amazonas, 69077-000, Manaus, AM, Brasil
[3]Departamento de Física, Universidade Federal de Sergipe, 49100-000, São Cristóvão, SE, Brasil
[4]Instituto Federal de Educação Ciência e Tecnologia do Amazonas, 69020-120, Manaus, AM, Brasil
[5] LPMAT, Departamento de Engenharia de Materiais, Universidade Federal do Amazonas, 69077-000, Manaus, AM, Brasil
[6]IFIMUP-IN, Institut of Nanoscience and Nanotechnology, Departamento de Física e Astronomia. Faculdade de Ciências da Universidade do Porto, 4169-007 Porto, Portugal

Abstract: The ceramic system $La_{2/3-x}Li_{3x}TiO_3$ presents as an interesting candidate to be used as an electrolyte in solid-state Li-ion batteries. In this paper the electrical response of the ceramic, $La_{2/3-x}Li_{3x}TiO_3$ with x = 0.11 is reported. $La_{2/3-x}Li_{3x}TiO_3$ nanoparticles were synthesized by high energy milling and sintered by Spark Plasma Sintering from an amorphous phase. After sintering, the samples were structurally characterized by XRD and Raman techniques. Measurements of complex impedance varying frequency from 1 Hz to 10 MHz and temperature from 25 °C to 270 °C were performed. The study of DC conductivity allowed us to find the contributions to the total conductivity, grain, and grain boundary of the samples. From the activation energy values, it was possible to determine the conductive mechanism corresponding to the mobility of Li^+ ions.

1 Introduction

Lithium-based batteries are energy sources that need to be studied and developed, taking into consideration, in addition to their efficiency, public and environmental safety issues. In this respect, organic liquid electrolyte batteries with lithium-ion (Li^+) carriers are flammable and susceptible to auto ignition, which may occur due to internal short circuit caused by physical damage after mechanical impact, heating at ambient temperatures, or internal manufacturing defect [1]. Incidents such as lithium-ion battery fires worry about the safety issue in personal electronics, transport vehicles, and commercial airplanes [2]. For this reason, it has been proposed to replace these types of batteries with electrolytes in the solid-state, since they present greater safety in such devices [3-5].

Some inorganic solid-state electrolytes have high ionic conductivity at room temperature (10^{-3} to 10^{-4} S/cm), as well as excellent chemical stability to the electrodes [1]. Other advantages of these electrolytes are: the reduction of heating of the batteries, longer durability, corrosion elimination, etc. Among the lithium-based solid-state electrolytes, lanthanum lithium titanate with perovskite structure (LLTO) has been extensively studied [6]. It has relatively high intrinsic ionic conductivity "dc" at room temperature, reaching values of up to 10^{-3} S/cm. The high conductivity values obtained from LLTO can be related to its open, stable and rigid crystalline structure, with holes and interstices accessible to the Li^+ ion; also, the small mass and size of the lithium-ion facilitate the electric conduction process [7].

It is a recognized fact that synthesis method is decisive to obtain a material with good properties. Among the most recently used techniques, for the synthesis of materials with a particle size of the order of nanometers, the mechanical activation or high energy grinding (MAE) [8] stands out. MAE has been pointed out as an inexpensive way to produce materials out of balance in the most varied forms. The final milling products are generally nanoscale and are characterized by a large surface area, high defect density, and higher diffusion rates [9].

The Spark plasma sintering (SPS) process offers several advantages over conventional methods, such as ease of operation, high sintering speed, high reproducibility, safety, reliability, as well as high-density values in the samples [10]. Recently the authors of this work reported the use of this method for LLTO samples with x = 0.08 [9].

This work has as main objective to characterize the electrical response of the ceramic system $La_{2/3-x}Li_{3x}TiO_3$ with x = 0.11 obtained by the combination of high energy ball milling and sintering via SPS. On the other hand, will be established a comparison with results previously reported by the authors.

2 Materials and Methods

$La_{2/3-x}Li_{3x}TiO_3$ nanopowders were synthesized by the high energy milling technique. The precursor materials, La_2O_3 (Aldrich - 99.9%), Li_2CO_3 (Aldrich - 99.9%) and TiO_2 (Aldrich - 99.7%) were subjected to a high energy milling process in a planetary mill. The sample was obtained by SPS following the same methodology used in the references [9,11].

The structural characterization of the samples was performed by X-ray diffraction (XRD) using a Rigaku D-max diffractometer in continuous mode from 10 to 90 ^{0} in 2θ and Cukα radiation. Another technique used for this purpose was Raman Spectroscopy using a Jobin-Yvon T64000 spectrometer. Measurements were performed with an Ar + 15 mW laser at room temperature using a 514.5 nm excitation line. Meanwhile, for the electrical characterization of the samples, the Complex Impedance Spectroscopy technique was used. Measurements were performed using a Solartron 1260 Impedance Analyzer. A potential of 0.5 V and a range of temperature and frequency of 25 to 270 ^{0}C and 100 Hz to 10 MHz, respectively, were used as measurement parameters. The structural and electrical characterization was similar to that used in reference [9].

3 Results and Discussion

Figure 1a shows the X-ray diffraction patterns of the ceramics $La_{2/3-x}Li_{3x}TiO_3$ doped with x = 0.11 after sintering and heat treatment. In this figure, a tetragonal structure with a spatial group P4 / mmm was identified as the main phase, similar to that reported by other authors

[12]. Additional peaks corresponding to a secondary phase were identified as $Li_4Ti_7O_{16}$. This structure was reported by BERTAUT in 1953 and there is no cif file of it, which makes refinement difficult. A slight variation in the position and intensity of the diffraction peaks can be reported in comparison with the reference [9] where the sample was studied with x = 0.08 Li^+ ions. This behavior may be motivated by an increase in Li^+ ion concentration in the crystalline structure of the material, which creates a larger number of point defects within the crystal structure of the LLTO.

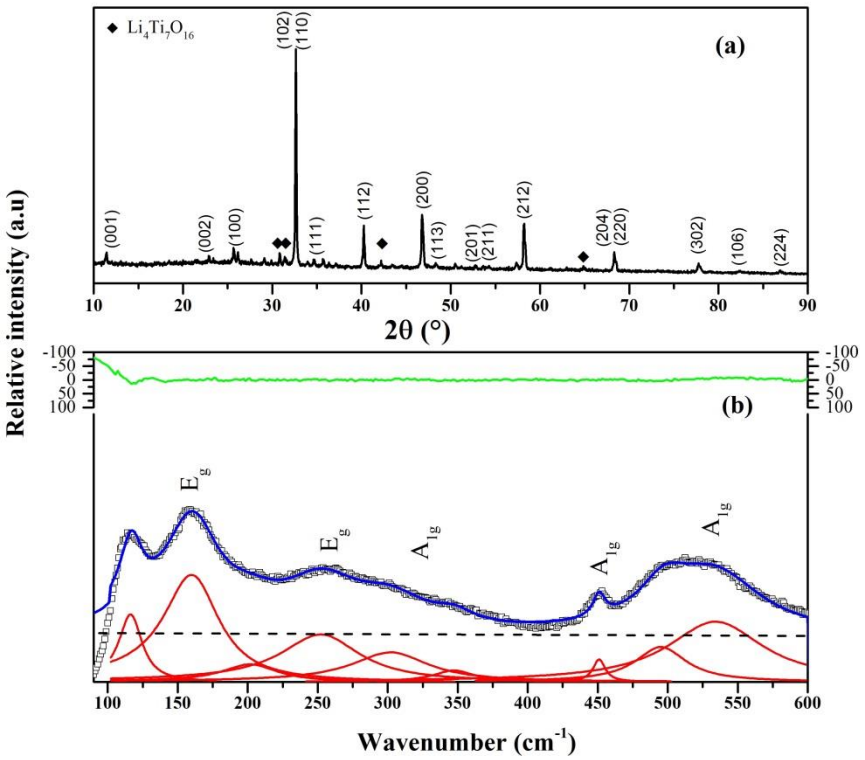

Figure 1. (a) X-ray diffraction patterns of the $La_{2/3-x}Li_{3x}TiO_3$ ceramics obtained by SPS, x = 0.11. The marked peaks (•) correspond to a secondary phase of $Li_4Ti_7O_{16}$. (b) Raman spectra of the $La_{2/3-x}Li_{3x}TiO_3$ ceramic with x = 0.11.

The Li^+ ions insertion into the crystalline structure of the samples was also corroborated by Raman vibrational spectroscopy. The Raman spectra at room temperature of the ceramics system are shown in Figure 1b.

The main Raman bands identified for the sample are similar to those reported in the literature and by the authors of this work [9,13]. The Raman spectra were fitted by oscillator functions with an IGOR PRO 6.0 program, where for 0.11 the bands were located at 163, 256 and 537 cm^{-1} with symmetry Eg were found, while bands 315, 448, 557 and 580 cm^{-1} were detected in the A1g modes. Thus, the band at 163 cm^{-1} is associated mainly with the cations of Ti, more precisely to the vibration of Ti in the plane. The 256 cm^{-1} band is associated with oxygen on the plane. The bands at 305 cm^{-1} are composed mainly of Ti-vibration along the c-axis and the 451 cm^{-1} bands pertained to along the axis c on oxygen (1, 2). The band at 537 cm^{-1} seems more likely to be due to O(3) on the plane. A summary of the observed bands is shown in Table 1. They are obtained from the best fit of the spectra.

The obtained Raman bands are compatible with the tetragonal structure P4/mmm, evidenced by the analysis of the X-ray pattern [9,12,13]. However, it is worth mentioning that Raman spectra present a displacement when compared with previously reported samples [9]. This behavior can be caused by a higher concentration of Li^+ ions in the crystalline structure of the samples; which should contribute to an increase in the number and density of point defects. A similar result was obtained in X-ray diffraction.

Table 1. Values obtained from the Raman spectra adjustments of the LLTO samples with x = 0.08 and x = 0.11.

*x = 0.08**	*x = 0.11*	*Symmetry*	*Atomic displacement*
118	117		
150	163	E_g	Ti - on the plan
178	215		
247	256	E_g	O(3) - on the plan
324	305	A_{1g}	Ti – along the axis c
389	348		
459	451	A_{1g} (prohibited)	O(1,2) – along the axis c
	498		
532	537	E_g	O(3) - on the plane
562		A_{1g} (permitted)	O(3) – along the axis c
589		A_{1g} (permitted)	O(3) – along the axis c

*Results of reference [9]

As it is known, the dopant elements introduction into the crystalline structure of the materials generates some changes in the physical properties. In the case of lithium content, this fact directly affects the structural properties and electrical characteristics of the LLTO system [13,14]. This work corroborates the above effect, showing the influence of the lithium content on the electrical properties of the LLTO system with x = 0.11.

Figure 2 shows the Nyquist plot of the LLTO system with x = 0.08 (white squares) and the sample x = 0.11 (black squares) at room temperature. Comparing the Nyquist plot of these samples similar behavior can be observed, without significant difference in their maximum values of the imaginary part of the impedance, independently of the lithium content. The window of the real part of the impedance also does not present change with the variation of the lithium content. For both cases, the obtained values are of the same order of magnitude. The same behavior for other temperatures was observed, showing that at least under the conditions that these tests were developed; there is no change in the electrical properties and specifically in the conductivity of the sample. Curves for temperature values are not other shown.

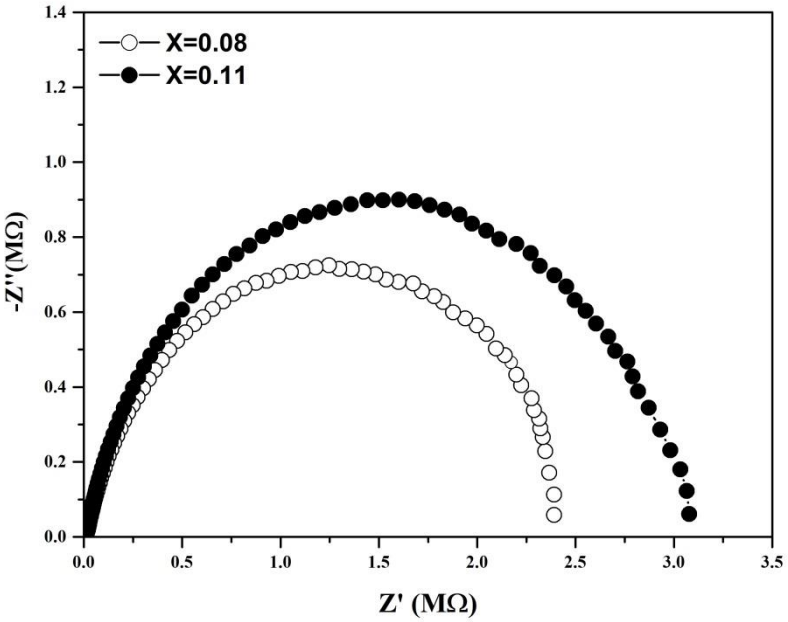

Figure 2: Comparison of the Nyquist plot at room temperature of the LLTO system with X = 0.08 and X = 0.11.

In a similar way to what was done in reference [9] the contributions of grain conductivity, grain boundary, and total conductivity were obtained. The EC (Equivalent Circuit) model was applied to the Nyquist plot of the sample with x = 0.11 to calculate the grain and grain boundary strengths. The circuit proposed to represent the behavior of the sample is the same as that used in reference [9].

Table 2. Conductivity of grain (σ_g), grain boundary (σ_{gb}) and total conductivity (σ_T) obtained via the CE model at different temperatures

T(°C)	*σ_g (S/cm)*	*σ_{gb} (S/cm)*	*σ_T (S/cm)*
25	2,54 x 10^{-05}	1,02 x 10^{-07}	3,33 x 10^{-07}
65	6.17 x 10^{-05}	1.35 x 10^{-07}	1.10 x 10^{-07}
90	1.48 x 10^{-04}	2.08 x 10^{-07}	1.87 x 10^{-07}
120	2.85 x 10^{-04}	5.92 x 10^{-07}	5.42 x 10^{-07}
150	4.5 x 10^{-04}	1.65 x 10^{-06}	1.51 x 10^{-06}
180	6.39 x 10^{-04}	4.01 x 10^{-06}	3.72 x 10^{-06}
210	7.96 x 10^{-04}	9.47 x 10^{-06}	8.78 x 10^{-06}
240	9.33 x 10^{-04}	1.98 x 10^{-05}	1.80 x 10^{-05}
270	1.09 x 10^{-03}	3.98 x 10^{-05}	3.69 x 10^{-05}

From the values of the resistance, calculated by the EC model, and the geometric factor of the sample, it was possible to obtain the values of the dc conductivity of the grain (σ_g) and its grain boundary (σ_{gb}). The total conductivity $\sigma_T = d/R_tS$, where d, R_t and S, are thickness (cm), total electrical resistance (Ω) and area of the sample (cm^2) are calculated from the total resistance, $R_t = R_g + R_{gb}$, respectively. Table 2 shows the values of the conductivity of the grain and grain boundary obtained using the EC model at different temperatures. As can be observed from 25 °C to 270 °C an increase in the dc conductivity values of the sample occurs. A similar behavior was reported in the reference [9].

On the other hand, it was not possible to detect a variation in conductivity values for this sample when compared to that reported in the reference [9]. To a large extent, this result can be strongly motivated by the presence of the secondary phase. This secondary phase reported by X-ray diffraction could be influencing the electrical conductivity of DC and even with the conductive mechanism itself.

The Arrhenius behavior of the sample under study (x = 0.11) is reported in Figure 2, where the values of the activation energies (Ea) of the contribution of the grain, its contour and total conductivities are shown. It is observed the same behavior reported in [9], where the total activation energy is very close to the activation energy of the grain boundary. Therefore, it can be concluded that the grain boundary has a determinant contribution to the results of the total DC conductivity of the sample. The activation energy values obtained for the grain, border, and total conductivities are similar to those already reported [9,12,15-17]. From this result it is possible to conclude that regardless of the influence on the total conductivity of the system, the conduction mechanism remains the same: Li^+ ion mobility is still present in these samples. Thus, the grain frontier governs the electric conduction process, with its more insulating character, which decreases with increasing temperature.

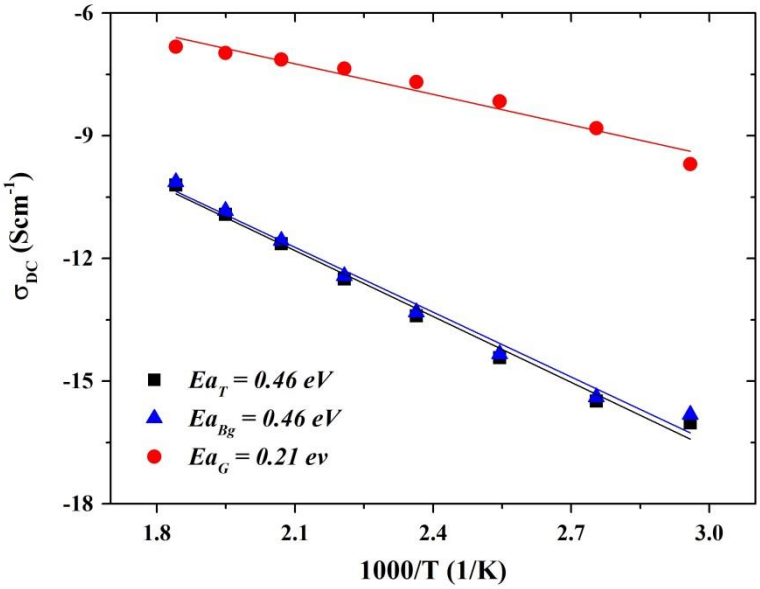

Figure 3. Arrhenius behavior of the grain, grain boundaries and total conductivities of the sample with x = 0.11, sintered via SPS.

4 Conclusions

The LLTO samples with x = 0.11 were made from high energy milling and sintered in the disk form, from a non-crystalline phase, by SPS. The obtained ceramics were characterized structurally, exhibiting a tetragonal phase, with the presence of a secondary phase, corresponding to $Li_4Ti_7O_{16}$. The model of the equivalent circuit was used successfully to obtain the conductivities of each region. From these values, the corresponding DC conductivity values were calculated. In this case, dc conductivity values between 10^{-5} to 10^{-3} S/cm^{-1} and 10^{-7} to 10^{-5} S/cm^{-1} are achieved for grain and grain boundary, respectively. This result evidenced a predominance of the isolating character of grain boundaries of those samples. From Arrhenius plot, the activation energy value for grain (0.214 eV), grain boundaries (0.455 eV), and total conductivity (0.462 eV) was determined. This result corroborates the existence of a conductivity mechanism by diffusion of Li^+ ions, through the crystalline structure of the material. Finally, the sample X = 0.11 did not show considerable improvements compared to the sample x = 0.08 previously reported.

Acknowledgments

The authors would like to thank to CNPq, FAPEAM and CAPES [N° 8454/2014-00] Brazilian and FCT [938/2016] Portuguese agencies for financial support. Finally, Mrs. Inmaculada Martinez, Ph.D Rosalia Poyato, Ph.D Angela Gallardo, for the great help in obtaining of the samples used in this work.

References

[1] F. Zheng, M. Kotobuki, S. Song, M.O. Lai, L. Lu, J. Power Sources **389**, 198 (2018)
[2] B. Zhang, R. Tan, L. Yang, J. Zheng, K. Zhang, S. Mo, Z. Lin, F. Pan, Energy Storage Mater **10**, 139 (2018)
[3] Y. Sun, P. Guan, Y. Liu, H. Xu, S. Li, D. Chu, Crit. Rev. Solid State Mater Sci **44**, 265 (2019)
[4] C. Sun, J. Liu, Y. Gong, D.P. Wilkinson, J. Zhang, Nano Energy **33**, 363 (2017)
[5] S. Chen, D. Xie, G. Liu, J.P. Mwizerwa, Q. Zhang, Y. Zhao, X. Xu, X. Yao, Energy Storage Mater **14**, 58 (2018)
[6] X. Hu, X. Cheng, S. Qin, G. Yan, J. Malzbender, W. Qiang, B. Huang, Ceram. Int. **44**, 1902 (2018)
[7] T. Šalkus, I. Steins, M. Barre, A. Kežionis, A.F. Orliukas, Mater Sci Medziagotyra **19**, 250 (2013)
[8] D. Xie, S. Chen, Z. Zhang, J. Ren, L. Yao, L. Wu, X. Yao, X. Xu, J. Power Sources **389**, 140 (2018)
[9] J.S. Pereira, F. Guerrero, Y. Romaguera-Barcelay, J. Anglada-Rivera, J.C.C. Sales, R.S. Silva, Y. Zulueta, R. Poyato, A. Gallardo, A. Almeida, A. Moreira, Y. Leyet, Mater. Res. Express **6**, 15504 (2019)
[10] H. Zhu, J. Liu, J. Power Sources **391**, 10 (2018)
[11] Y. Leyet, F. Guerrero, J. Anglada-Rivera, I. Martinez, H. Amorin, Y. Romaguera-Barcelay, R. Poyato, A. Gallardo-Lopez, Ferroelectrics **498**, 62 (2016)
[12] T. Yang, Y. Li, C.K. Chan, J. Power Sources **287**, 164 (2015)

[13] M. Romero, R. Faccio, S. Vázquez, S. Davyt, Ceram. Int **42**, 15414 (2016)
[14] Q. Wang, J. Zhang, X. He, G. Cao, J. Hu, J. Pan, G. Shao, J. Eur. Ceram. Soc **39**, 3332 (2019)
[15] H. Geng, A. Mei, Y. Lin, C. Nan, Mater. Sci. Eng. B Solid-State Mater. Adv. Technol **164**, 91 (2009)
[16] T. Šalkus, E. Kazakevičius, A. Kežionis, A.F. Orliukas, J.C. Badot, O. Bohnke, Solid State Ionics **188**, 69 (2011)
[17] C. Uhlmann, P. Braun, J. Illig, A. Weber, E. Ivers-Tiffée, J. Power Sources **307**, 578 (2016)